Evaluation of Solar Pool Heating System Under Different Conditions

Sebastian Pater * and Krzysztof Kupiec *

Posted Date: 25 March 2026

doi: 10.20944/preprints202603.1893.v1

Keywords: outdoor pool heating; climatic conditions; solar heating system

 doi:10.20944/preprints202603.1893.v1

Article

Evaluation of Solar Pool Heating System Under Different Conditions

Sebastian Pater * and Krzysztof Kupiec *

Faculty of Chemical Engineering and Technology, Cracow University of Technology, Warszawska 24 St, 31-155 Krakow, Poland

* Correspondence: sebastian.pater@pk.edu.pl (S.P.); krzysztof.kupiec@pk.edu.pl (K.K.)

Abstract

Heating water in outdoor pools is common, particularly in regions with cool or temperate climates. Several factors, including solar radiation, ambient air temperature, wind speed, and humidity, influence the pool water temperature. A key design challenge is to determine the collector surface area required to achieve the desired pool water temperature. In this study, a mathematical model was developed that accounts for the aforementioned factors. Under various operating conditions, thermal performance calculations were carried out. Climatic conditions at three locations across Europe, representing different climate regimes, were analyzed. The model was validated through comparison with results obtained in the POLYSUN simulation software. The calculations demonstrated that wind speed above the water surface has a significant impact on heat losses and, consequently, on water temperature. It causes both convective and evaporative heat losses. Locating the pool in a sheltered area results in a consistent reduction in heat losses. It was determined that, under the climatic conditions of Krakow, the installation of solar collectors with a surface area equal to 50 % of the pool surface enables the maintenance of daytime water temperatures above 21 °C for approximately 100 days. In the absence of solar collectors, achieving such temperatures is not feasible.

Keywords: outdoor pool heating; climatic conditions; solar heating system

1. Introduction

Solar energy constitutes a sustainable and economically viable solution for low-temperature heat applications, including swimming pool heating. Given the relatively moderate temperature levels required and the strong coincidence between solar availability and pool usage periods, solar thermal systems are particularly well-suited for this purpose. In summer, solar energy can be used to heat the pool water, thereby mitigating the problem of surplus thermal energy produced by solar collectors. Swimming pools experience significant and persistent heat losses driven by evaporation, convective heat transfer, long-wave radiation flux, which leads to continuous heating demand. As a result, their specific energy consumption is often considerably high, making them a critical target for energy efficiency improvements and the integration of renewable energy technologies [1,2]. In this context, the decarbonization of pool heating systems is essential not only to reduce greenhouse gas emissions but also to limit long-term operational costs.

Solar thermal heating systems are mature, energy-efficient technology for swimming pool applications, particularly in outdoor and semi-open configurations. Their straightforward integration with existing hydraulic and filtration systems, combined with their ability to reduce auxiliary energy demand significantly, makes them a key strategy for lowering fossil fuel dependency. A comprehensive state-of-the-art review by Li et al. [3] indicates that unglazed solar collectors are frequently employed in such applications due to their high efficiency under low temperature differences, low investment cost, and simple operation. Nevertheless, the actual performance of solar pool heating systems is strongly influenced by climatic conditions, system configuration, collector type, and control strategies. Parameters such as solar irradiance, ambient temperature, wind speed,

 doi:10.20944/preprints202603.1893.v1

and humidity directly affect both heat gains and losses, and consequently determine the achievable solar fraction and seasonal efficiency.

Several experimental and numerical studies have demonstrated the technical feasibility and energy benefits of solar pool heating systems. Ruiz and Martínez [4] developed a TRNSYS model validated with experimental data for an outdoor swimming pool and showed that solar systems can supply a large share of annual heating demand when properly sized. Similarly, Lugo et al. [5] combined numerical simulations with experimental validation for warm climates, highlighting the strong influence of collector area, mass flow rate, and control strategies on system efficiency.

Hydraulic parameters and control strategies have been identified as key factors in optimizing system performance by Zhao et al. [6]. They experimentally showed that reducing flow rate and pump speed improves collector efficiency while lowering electricity consumption. These results were confirmed by Cunio and Sproul [7], who reported enhanced energy savings and thermal efficiency for unglazed solar collectors operating under reduced flow conditions.

Analysis of solar heating of swimming pools using the utilizability method was presented in the article [1] by Gonçalves et al. This approach allows the evaluation of solar energy contribution under varying climatic and operational conditions. The study demonstrates that the utilizability method, similarly as presented in the article [8], is an effective tool for optimizing solar thermal system design and predicting energy savings in pool heating applications. Simulations were performed for several locations in Brazil. The solar fraction values were determined under the following conditions: a pool surface area of 250 m², a collector surface area of 150 m², and a water temperature of 30 °C.

Beyond conventional solar thermal systems, hybrid solutions have received increasing attention. Solar-assisted heat pump systems have been investigated by Starke et al. [9] and Li et al. [10], who demonstrated that the integration of solar collectors with heat pumps and thermal energy storage significantly improves seasonal performance. Similar conclusions were drawn by Ren et al. [11], who showed that hybrid thermal energy storage enhances operational stability and reduces auxiliary energy use. Sezen and Gungor [12] further confirmed through a comparative review that solar-assisted heat pump systems outperform standalone systems in terms of efficiency.

More recently, integrated photovoltaic/thermal systems have been proposed for pool heating applications. Luo et al. [13] experimentally and theoretically analyzed a solar PV/T pool system and demonstrated that simultaneous heat and electricity generation can significantly improve overall system efficiency. At a real scale, Katsaprakakis [14] reported the successful implementation of a solar-combi system for swimming pool heating and domestic hot water production in Greece, achieving substantial fossil fuel savings.

From an economic and sustainability perspective, Mardi El et al. [15] conducted a life-cycle cost of heat assessment and showed that solar thermal collectors and PV-assisted heat pump systems represent some of the most cost-effective and environmentally sustainable solutions for indoor swimming pools. However, their performance and economic viability are highly sensitive to local climatic conditions and energy prices.

Water in open reservoirs generally has a lower temperature than the surrounding air due to heat losses caused, among other factors, by evaporation. In high-latitude countries, solar energy alone is often insufficient to maintain a comfortable water temperature in outdoor pools, which necessitates additional heating. Water heating is also commonly used in warm-climate countries to extend the swimming season. Due to the high cost of heating with conventional energy sources, solar energy is widely used for heating outdoor pools. The use of heat pumps is also a beneficial solution. However, this does not necessarily mean abandoning solar energy, which can significantly support the operation of heat pumps. Solar heating of outdoor pools is a very cost-effective method, particularly when simple unglazed solar collectors are used, directly connected to the pool heat system.

Pool water temperature is governed by multiple interacting factors, such as solar radiation, ambient air temperature, wind speed, humidity, and the surface area of installed solar collectors. In this study, a mathematical model was developed that incorporates these variables by dividing the daily cycle into two distinct periods, daytime and nighttime, defined by sunrise and sunset. When

 doi:10.20944/preprints202603.1893.v1

combined with the concept of utilizability, this approach yields a relatively simple model that provides an adequate representation of the real process. Thermal performance was evaluated under a range of operating conditions. Furthermore, achievable water temperatures under different climatic conditions in three European cities were analyzed: Thessaloniki, Krakow, and Stockholm. These cities are located near the 20°E meridian and at latitudes of 40°, 50°, and 60°N, respectively. Simulations were conducted to assess the maximum pool water temperature at these locations assuming identical collector and pool surface areas. The calculations were performed using the proposed model and the POLYSUN simulation software.

2. Mathematical Model of the Process

2.1. Installation Scheme

A simplified scheme of a solar water heating system for a swimming pool is shown in Figure 1. In the system presented in Figure 1a, solar heat is supplied directly to the water flowing in the pool-pump-collector loop (filtering and control devices are not depicted). Assuming perfect mixing of the water in the pool and ignoring heat losses in the pipes, the temperature at the collector inlet is equal to the temperature of the water in the pool T_p.

Figure 1b presents an installation with a coil placed in a pool where the T_p remains constant regardless of position. The temperature at the outlet of the heat exchanger T_p' (equal to the temperature at the inlet to the collector) is lower than T_p in this case. The following relationship is valid [16]:

$$\frac{T_c - T_p'}{T_c - T_p} = 1 - \exp(-NTU) \tag{1}$$

where the number of transfer units (NTU) is defined as follows:

$$NTU = \frac{(UA)_{HEX}}{\dot{m}_{HEX} c} \tag{2}$$

where U is the overall heat transfer coefficient, A is the heat exchanger surface, $\dot{m}_{HEX}$ is the water flow rate in heat exchanger, and c is the water heat capacity.

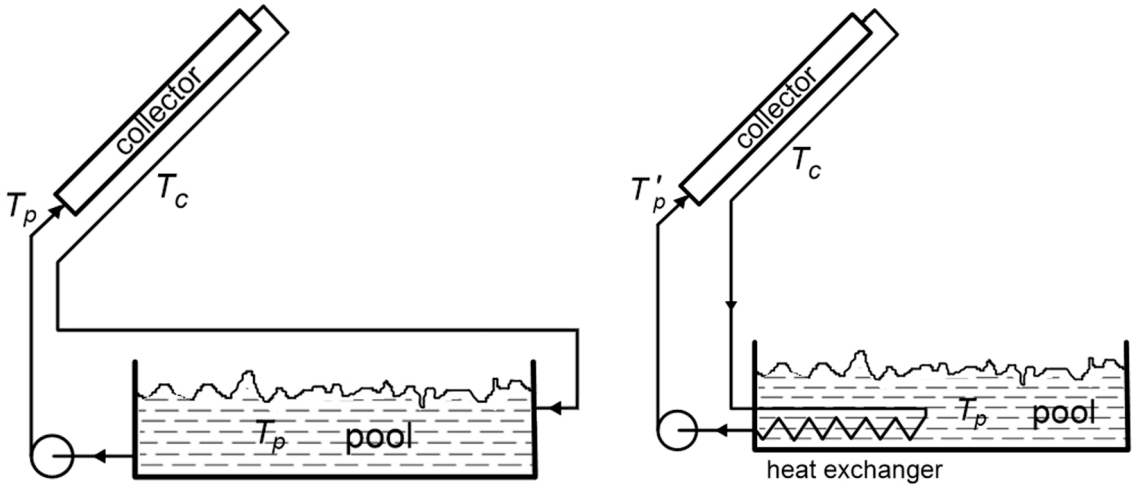

(**a**) without heat exchanger (**b**) with heat exchanger

Figure 1. Solar water heating in swimming pools.

2.2. Modeling Daily Changes of Insolation and Temperature

One way to model processes involving solar radiation is to use instantaneous data (e.g., hourly), which accurately reflects actual weather changes. However, a disadvantage of this calculation method is that the generated curves of process parameter variations correspond only to the specific

 doi:10.20944/preprints202603.1893.v1

time period represented by the weather data used. Therefore, they cannot be treated as generalized curves.

Another option is to use data that has been averaged according to certain rules. For seasonal or annual calculations, data for a typical meteorological year can be used. Such data can be processed numerically by developing functions that approximate the values of individual variables over time (e.g., ambient temperature, solar radiation, clearness index). The disadvantage of this method of calculation is that such approximations generally do not apply to hourly values, as the approximation functions would then be too complex. Using average daily weather data can lead to significant errors, as it assumes, among other things, that the intensity of solar radiation is the same during the day and at night.

To avoid the disadvantages of both methods, this study uses a compromise model based on dividing each day into two periods, conventionally referred to as day (D) and night (N), separated by sunrise and sunset. The method for determining the length of daytime and nighttime hours and air temperature T_a for individual days and nights is as follows. The input data for individual days of the year are the average daily air temperature T_a and the daily insolation on the collector surface H_T. The length of the day Δt_d (in hours) is calculated according to the relationship [17]:

$$\Delta t_d = \frac{24}{\pi} \cdot \mathrm{abs}(\omega_s) \tag{3}$$

where sunset (or sunrise) hour angle ω_s is calculated using the following formula [17]:

$$\omega_s = \arccos\big(-\tan(\psi)\big) \cdot \tan(\delta) \tag{4}$$

where declination δ was determined from:

$$\delta = 23.45 \cdot \frac{\pi}{180} \cdot \sin\left(\frac{2\pi}{365}(284 + n)\right) \tag{5}$$

Knowing the length of the day, it is easy to determine the beginning and end time of the daily period t_1 and t_2:

$$t_1 = 12 - \Delta t_d/2 \tag{6a}$$

$$t_2 = 12 + \Delta t_d/2 \tag{6b}$$

For a given H_T value, the average daily insolation relative to the length of day period is equal to:

$$H_{Td} = \frac{24}{\Delta t_d} \cdot H_T \tag{7}$$

whereas at night $H_{Tn} = 0$ which is graphically presented in Figure 2.

To determine the average air temperatures during the day T_d and at night T_n period, the daily temperature profile must be estimated. The daily air temperature profile was approximated by the following relationship:

$$T = T_a - B_d \cos(\omega_d t) \tag{8}$$

where B_d is the daily temperature amplitude, and ω_d is the frequency (= 2π/24).

T_d and T_n were calculated as the integral averages of function (6) within the limits marked in Figure 3. The following results were obtained:

$$T_d = T_a - \frac{B_d}{\omega_d \cdot \Delta t_d}[\sin(\omega_d t_2) - \sin(\omega_d t_1)] \tag{9a}$$

$$T_n = T_a - \frac{B_d}{\omega_d \cdot (24 - \Delta t_d)}\big[\sin\big(\omega_d (t_1 + 24)\big) - \sin(\omega_d t_2)\big] \tag{9b}$$

 doi:10.20944/preprints202603.1893.v1

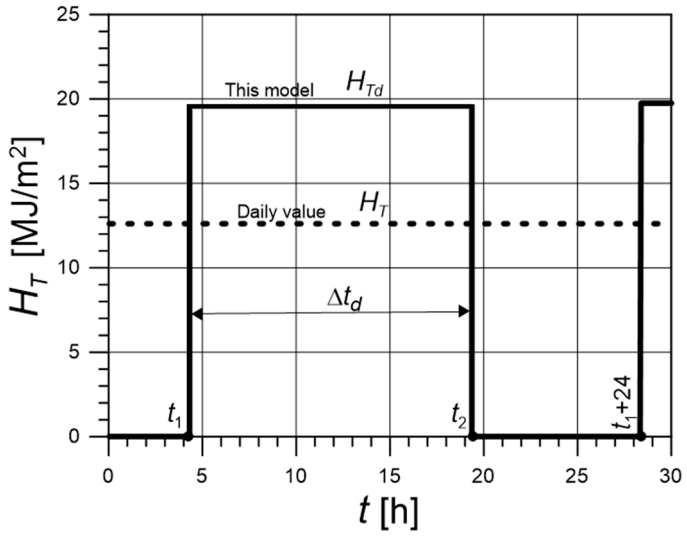

Figure 2. H_T and H_{Td} for the 135th day of the year.

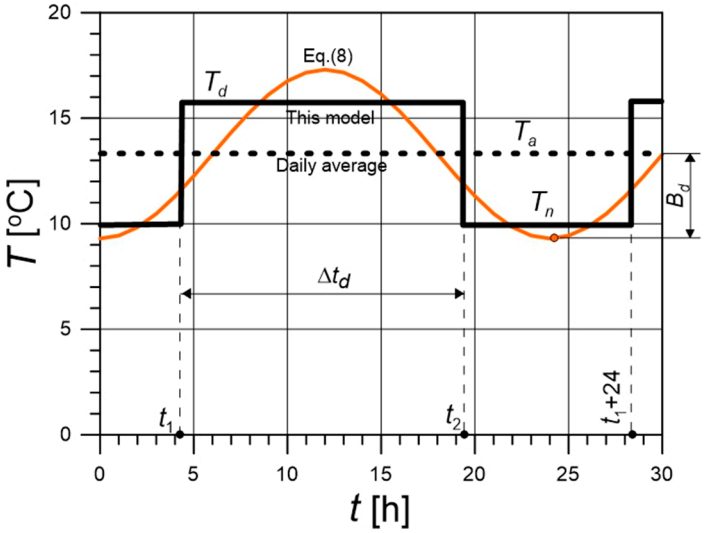

Figure 3. Time courses of T_a, T_d and T_n for the 135th day of the year.

The interpretation of average temperature and solar radiation values for the day and night periods is presented in Figures 3 and 4. The graphs correspond to the 135th day of the year (May 15). A value of B_d = 4 K was assumed. According to weather data for that day, the calculated values are: H_T = 12.7 MJ/m² and T_a = 13.3 °C. Δt_d is equal to 15.3 h, which results in t_1= 4.3 h and t_2= 19.3 h. The average day period temperature, i.e., between 4.3 h and 19.3 h, calculated from Eq. (9a), is T_d = 15.4°C. The average night period temperature, i.e., between 19.3 h and 4.3 (+24) h, according to Eq. (9b), is T_n = 10.1°C.

 doi:10.20944/preprints202603.1893.v1

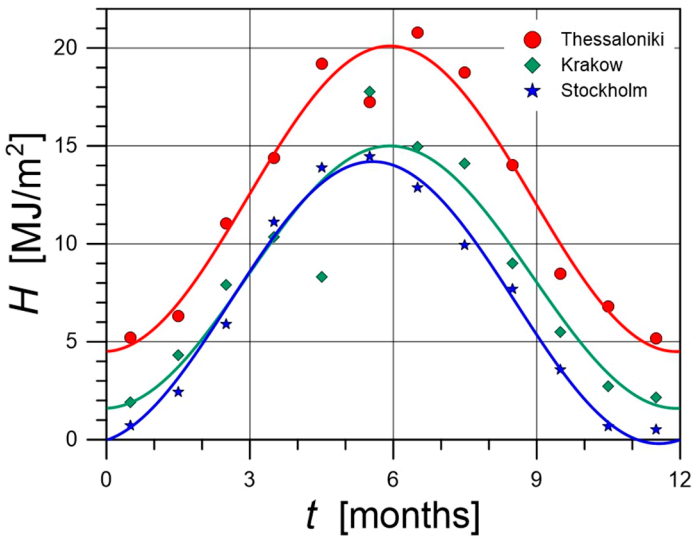

Figure 4. Time course of H in various locations.

2.3. Climate Parameters

Climatic conditions at three European locations representing different climate regimes, specifically Thessaloniki, Kraków, and Stockholm, were analyzed. The weather data for these locations were obtained from the Photovoltaic Geographical Information System (PVGIS) [18]. Typical meteorological year data for the period PVGIS-ERA5: 2005-2023 were used. The following parameters were considered: daily radiation on the horizontal surface H, T_a, relative air humidity RH, and wind speed u. Variations in RH and u are irregular throughout the year; therefore, average values were used. These values are presented in Table 1.

Table 1. Average annual values of RH and u.

	Thessaloniki	**Krakow**	**Stockholm**
RH	0.64	0.77	0.75
u [m/s]	4.4	2.3	3.1

The clearness index is defined as the ratio:

$$K_T = \frac{H}{H_0} \tag{10}$$

As can be seen in Figures 4–6, the time courses of H, RH, and K_T in each of the locations considered show regularity. The following relationship was used to approximate the data:

$$Y(t) = A - B \cdot \cos(\omega t - P_s) \tag{11}$$

where A, B, P_s are constants, and $\omega = 2\pi/365$. Table 2 presents the coefficient values used in Eq. (11) to calculate H, T_a, and K_T for individual locations.

 doi:10.20944/preprints202603.1893.v1

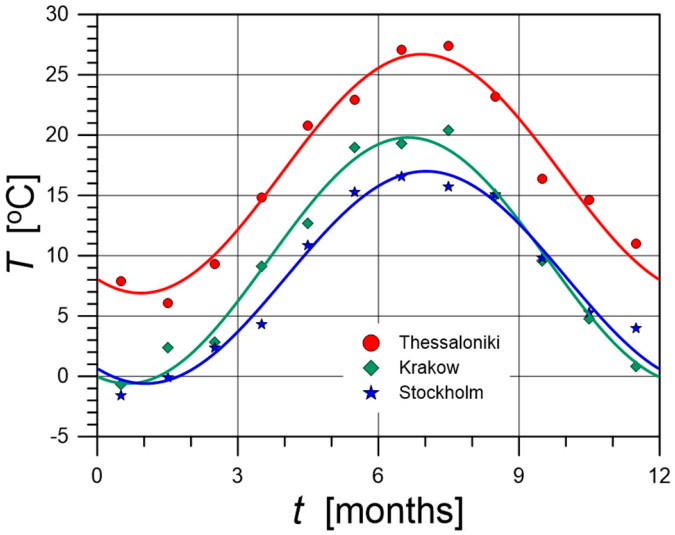

Figure 5. Time courses of T_a in various locations.

The daily insolation on the titled collector surface is calculated using the following formula:

$$H_T = R \cdot H \tag{12}$$

In this equation, R is the daily heat transfer from the horizontal surface to the inclined surface. The value of R refers to the total radiation and is calculated from equation:

$$R = \left(1 - \frac{H_d}{H}\right) R_b + \left(\frac{H_d}{H}\right)\left(\frac{1 + \cos\beta}{2}\right) + \rho_g \left(\frac{1 - \cos\beta}{2}\right) \tag{13}$$

Table 2. Coefficients for determining approximation relationships for H, T_a, and K_T.

		Thessaloniki	Krakow	Stockholm
H [MJ/m^2]	A	12.3	8.3	7.0
	B	7.8	6.7	7.2
	P_s	−0.03	−0.03	−0.22
T_a	A	16.8	9.6	8.2
	B	9.9	10.2	8.8
	P_s	0.49	0.34	0.54
K_T	A	0.418	0.321	0.626
	B	0.077	0.069	−0.146
	P_s	−0.62	−0.74	−0.05

 doi:10.20944/preprints202603.1893.v1

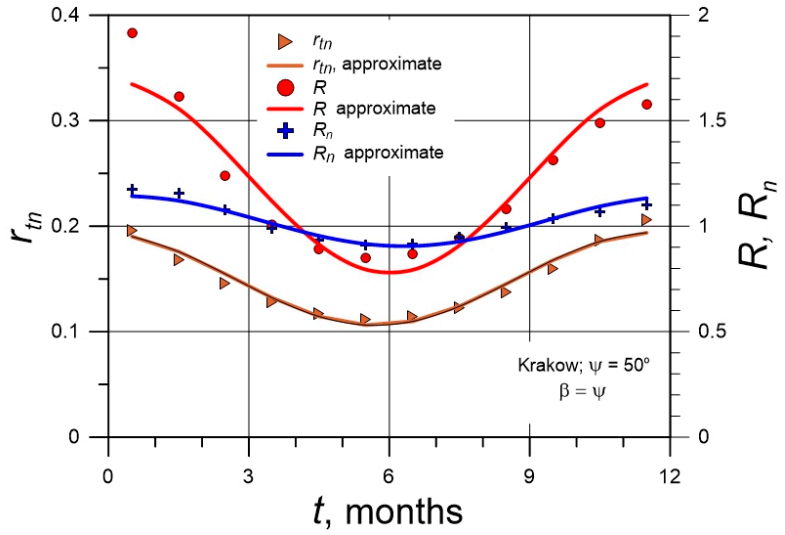

Figure 6. Time courses of R, R_n, and $r_{t,n}$ under the climatic conditions of Krakow.

The individual components in Eq. (13) denote direct radiation, diffuse radiation, and reflected radiation, respectively. The share of diffuse radiation $\frac{H_d}{H}$ can be determined based on empirical relationships as a function of the clearness index K_T. R_b is the ratio of daily beam radiation on a tilted surface to that on a horizontal surface and is a function of ψ and β. Figure 6 shows the time curves of the R coefficient under the climatic conditions of Krakow. ρ_g = 0.2 was assumed. Time courses shown were approximated using the periodic function given in Eq. (11). The determined coefficients A, B, and P_s are presented in Table 3.

Table 3. Approximation of R coefficients.

	Thessaloniki, $\psi = 40^\circ$	**Krakow, $\psi = 50^\circ$**	**Stockholm, $\psi = 60^\circ$**
A	1.175	1.233	1.501
B	−0.365	−0.455	−0.762
P_s	−0.08	0	−0.17

2.4. Utilizability

The model uses the concept of daily solar utilizability ϕ. It is defined as the ratio of usable energy obtained during the day to the total solar energy incident on the solar collector during the same period. ϕ considers the fact that some of the solar energy is not used when the radiation flux is lower than the heat flux lost from the collector to the environment. The critical solar radiation intensity I_{Tc} plays a key role, as it is the radiation intensity below which collectors do not supply heat to the system. From the definition of I_{Tc}, the following relationship follows:

$$I_{Tc} = \frac{U_L(T_p - T_a)}{(\tau\alpha)} \tag{14}$$

The value of ϕ therefore depends on I_{Tc} and indirectly on the inlet temperature of the collector. ϕ should be calculated according to the following equation [17]:

$$\phi = \exp\left\{\left[a + b\left(\frac{R_n}{R}\right)\right](X_c + cX_c^2)\right\} \tag{15}$$

where a, b, and c are constants dependent on K_T. Thus, the utilizability method is based on the correlation of ϕ with K_T, the ratio R_n/R, and the dimensionless critical radiation X_c defined as follows:

 doi:10.20944/preprints202603.1893.v1

$$X_c = \frac{I_{Tc}}{r_{t,n} R_n H} \tag{16}$$

The monthly average ratio of total radiation on the tilted plane to that on the horizontal plane R_n and ratio of total radiation in an hour to total in a day (noon) $r_{t,n}$ appearing in Eq. (15) and (16) are functions of time and angles:

$$R_n = f_1(t, \psi, \beta) \tag{17}$$

$$r_{t,n} = f_2(t, \psi) \tag{18}$$

The use of the utilizability method requires that the critical radiation level remains approximately constant. In practice, this occurs in systems with very large storage tanks or in systems without storage, where the medium entering the collector comes from a source with a constant temperature. Therefore, the concept of utilizability can be used in modeling solar water heating in a swimming pool.

Figure 6 shows examples of the time courses of the R_n and $r_{t,n}$. The shape of these profiles provides the basis for their approximation by a relationship given in Eq. (11). The constants obtained are presented in Table 4.

Table 4. Approximation of R_n and $r_{t,n}$ coefficients using the utilizability method.

	Thessaloniki, $\psi = 40^\circ$			**Krakow, $\psi = 50^\circ$**			**Stockholm, $\psi = 60^\circ$**		
	A	B	P_s	A	B	P_s	A	B	P_s
R_n	1.045	−0.108	0.06	1.025	−0.120	0.16	1.494	−0.553	−0.120
$r_{t,n}$	0.145	−0.029	−0.16	0.149	0.044	−0.16	0.163	−0.079	−0.16

2.5. Heat Transfer between the Water Surface and the Environment

Heat is transferred between the surface of the water in the pool and the surrounding environment because of convection, radiation, and evaporation. The convective heat flow H_{conv} is described by the following equation:

$$H_{conv} = h(T_p - T_a) \tag{19}$$

The heat transfer coefficient between the water surface and the environment h depends primarily on the wind speed above the water surface. There are numerous empirical equations for determining the value of h. The following relationship is often used [19]:

$$h = 3.1 + 2.1 \cdot u \tag{20}$$

In the installation discussed, there are two different radiation fluxes between the surface of the water in the pool and the surroundings: solar radiation (shortwave) flux and longwave radiation flux LW. The solar radiation flux was discussed in subsection 2.3. LW is directed opposite to the solar radiation flux: from the water surface to the sky. It can be described by the Stefan-Boltzmann equation:

$$LW = \varepsilon\sigma(T_p^4 - T_{sky}^4) \tag{21}$$

where ε is the emissivity of the water surface, σ is the Stefan-Boltzmann constant, and T_{sky} is the temperature of the sky. T_{sky} depends on T_a and RH. According to ASHRAE [19], it can be determined as follows:

$$T_{sky} = T_a - (1105.8 - 7.562 \cdot T_a + 0.01333 \cdot T_a^2 - 31.292 \cdot RH + 14.58 \cdot RH^2) \tag{22}$$

where in this equation T_a is in K.

The heat flux resulting from water evaporation EV is related to phase change. The difference in partial pressures of water vapor at the water surface and in the air causes the transport of water in

 doi:10.20944/preprints202603.1893.v1

the vapor form. With the transfer of the material component, heat is transported from the water surface to the air. Using the analogy between heat and mass transport to calculate the rate of water vapor transfer, the relationship describing the heat flux associated with evaporation can be determined as follows [19]:

$$EV = A\,(P_{sat} - p) \cdot h \tag{23}$$

where A is a constant defined in the following way:

$$A = \frac{LM_w}{PM_a c} \cdot \left(\frac{a}{D}\right)^{-2/3} \tag{24}$$

where L is heat of vaporization of water, M_a = 0.029 kg/mol and M_w = 0.018 kg/mol are in sequence molar masses of air and water, D = 22.5 · 10^{-6} m^2/s is the diffusion coefficient of water in air, c = 1010 J/(kg·K) is heat capacity of air, and a = 19.4 · 10^{-6} m^2/s is thermal diffusivity of air [20]. For a pressure P = 1 · 10^5 Pa, A = 0.0168 K/Pa was obtained [21].

2.6. Calculation Algorithm

The heat balance of the water in the pool is as follows. The amount of solar heat supplied to the water in the pool during the day Q_{in} was calculated from:

$$Q_{in} = Q_p + HA_p \tag{25}$$

where daily useful heat transferred to the pool system Q_p was obtained from:

$$Q_p = A_c F_R (\tau\alpha) H_T \phi \tag{26}$$

where F_R is the collector heat removal factor and $(\tau\alpha)$ is the effective transmittance–absorptance product.

The water in the pool losses heat Q_{out} through LW, EV and H_{conv}. The value of Q_{out} depends on the surface area of the water in the pool A_p and the time interval Δt and can be determined from the equation:

$$Q_{out} = (LW + EV + H_{conv}) \cdot A_p \cdot \Delta t \tag{27}$$

The calculations were performed alternately for night and day periods of individual days. For both periods, the calculations are iterative. The calculation algorithm for a single day is as follows. For the night period, Q_{in} = 0. Additionally, a tentative value of T is assumed. On this basis, H_{conv}, EV, T_{sky}, and LW are calculated substituting average ambient temperature for night T_{an} in each case. Then, Q_{out} and finally the water temperature at the end of the night period were calculated:

$$T_p = T_{p0} + \frac{Q_{in} - Q_{out}}{V_p \rho c} \tag{28}$$

where T_{p0} is the water temperature at the end of the daily period on the previous day. If f = Abs $(T_p - T)$ is less than ε, which characterizes the accuracy of the calculations, then $T_{pn} = T_p$. Otherwise, the calculations should be continued until the problem can be reduced to solving a nonlinear equation $f(T) = 0$.

For the daily period, a tentative value of T should be also assumed. Then, H_{conv}, EV, T_{sky}, and LW are calculated substituting ambient temperature for day T_{ad}. In the next step, determine ϕ and Q_p, followed by Q_{in} and Q_{out}. Ultimately, the water temperature at the end of the day period is calculated using the Eq. (28) where T_{p0} should be replaced with the temperature at the end of the night period T_{pn}. The temperature at the end of the day period is calculated by solving the nonlinear equation $f(T) = 0$, similarly to the night period.

3. Modeling Using the POLYSUN Software

 doi:10.20944/preprints202603.1893.v1

A schematic diagram of a pool solar water heating system generated in POLYSUN software version 2026.2 [22] is shown in Figure 7. The main component of the installation is an unglazed solar collector field that directly transfers the generated solar heat to an open pool without the use of an intermediate heat exchanger. This approach minimizes additional thermal losses associated with heat exchangers and eliminates various issues related to the use of different heat transfer media. The thermal performance of the solar collectors is calculated in accordance with the internationally recognized ISO 9806 standard. Water heated by the collectors circulates directly into the open pool. Pump operation is controlled by a differential temperature controller, which activates the pump when the collector outlet temperature exceeds the pool water temperature by a predefined threshold, thereby ensuring efficient heat gain. A fixed solar fluid flow of 30 l/min/m^2 was set. The fraction of the local wind speed affecting the collector array was set to 50 %. Similarly to the numerical model presented in Chapter 3, no heat losses in the pipelines were assumed.

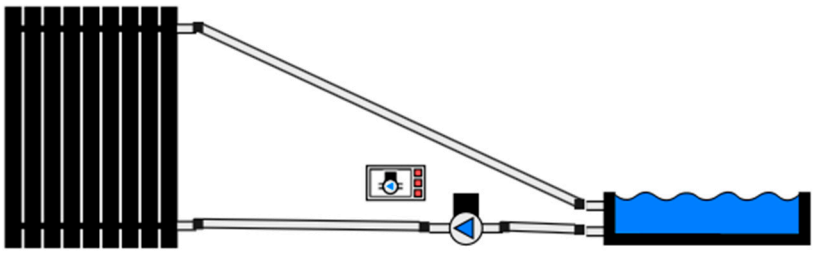

Figure 7. Schematic diagram of pool solar water heating system simulated in POLYSUN.

In the POLYSUN program, climate data are generated by default using the Meteonorm climate database (version 7.2). However, in the analyzed installation, more up-to-date climate data from the PVGIS database (PVGIS-ERA5, 2005–2023) [18] were used for the selected locations by implementing new data profiles in the program's source directory.

For the pool, an absorbance (i.e., the percentage of global radiation absorbed by the pool water) of 60 % was assumed, in accordance with the data presented by Duffie and Beckman [17]. Additionally, a solar radiation reflection of 8% at the water surface was considered.

4. Calculation Results

4.1. Comparison of the Proposed Model with the Results Obtained from the POLYSUN Application

The results of the calculations based on the model presented in Chapter 2 were compared with the results obtained using the POLYSYUN software. The comparison was carried out for various climatic conditions. An overview of the most important process parameters values used in the calculations are presented in Table 5.

Table 5. The process parameters values used in the calculations.

Parameter	Value
Diffuse reflectance, ρ_g	0.2
Pool surface area, A_p	24 m^2
Pool deep, h_p	1.35 m
Solar collector efficiency, $F_R(\tau\alpha)$; η_0	0.9 [1]
Solar collector heat losses coefficient, $F_R U$; a_1	21 W/(m^{2}K) [1]
Solar fluid heat capacity, c	4190 J/(kgK)
Solar fluid density, ρ	1000 kg/m^3
Solar fluid flow rate, $\dot{m}_p$	30 l/min/m^2

 doi:10.20944/preprints202603.1893.v1

The results of the calculations, illustrating the relationship between T_p and time, are presented in Figures 8–10. The curves generated by the proposed model are based on smoothed weather data; therefore, as they do not account for diurnal variations, they appear smooth, in contrast to the curves obtained from the POLYSUN application, which are based on hourly data. Taking this into account, the model reproduces the actual process trend correctly, albeit with limited accuracy.

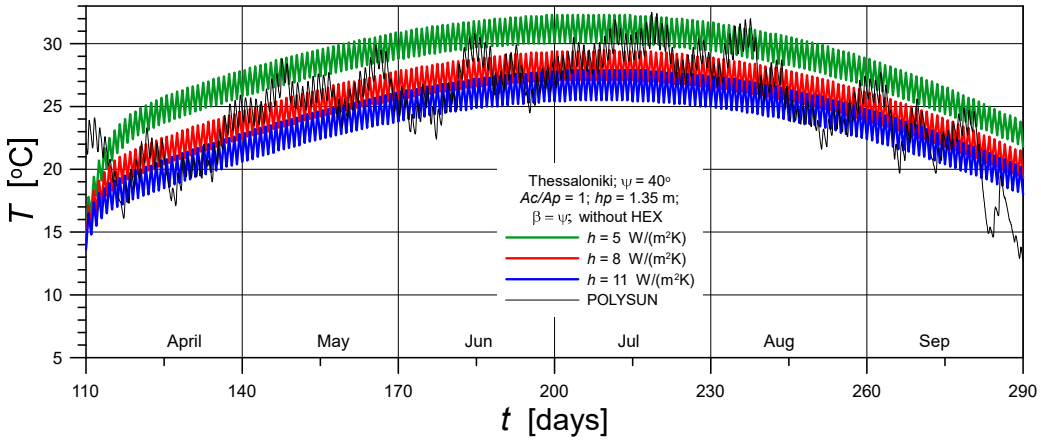

Figure 8. Time curves of T_p calculated by the proposed model and POLYSUN for Thessaloniki.

The curves in Figures 8–10 correspond to different values of h between the water surface and the environment. T_p strongly depends on the value of this coefficient. At the same time, h depends on u, which varies irregularly during the summer months. This variability makes it difficult to achieve full consistency between the temperature values obtained from the compared models. The temperature curves in the figures show that the difference in average water temperatures between day and night is, on average, 2–3 K, both for calculations based on the presented model and for those based on the POLYSUN application.

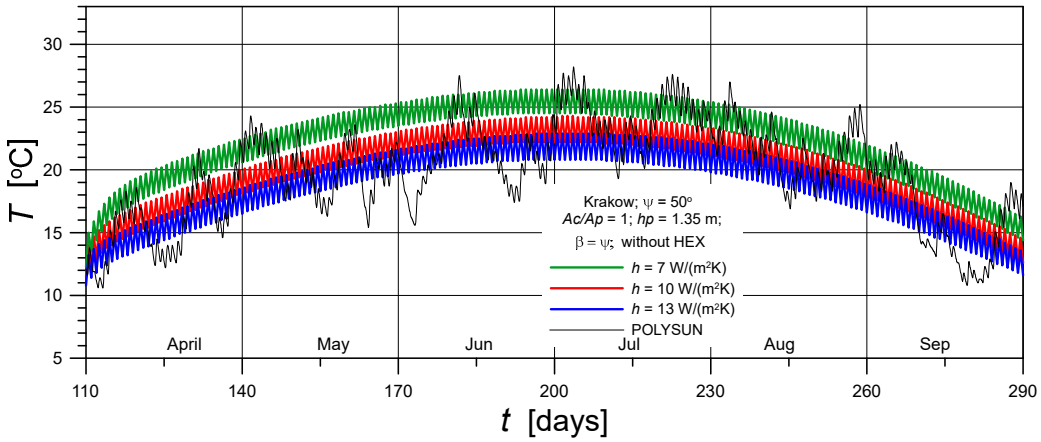

Figure 9. Time curves of T_p calculated by the proposed model and POLYSUN for Krakow.

 doi:10.20944/preprints202603.1893.v1

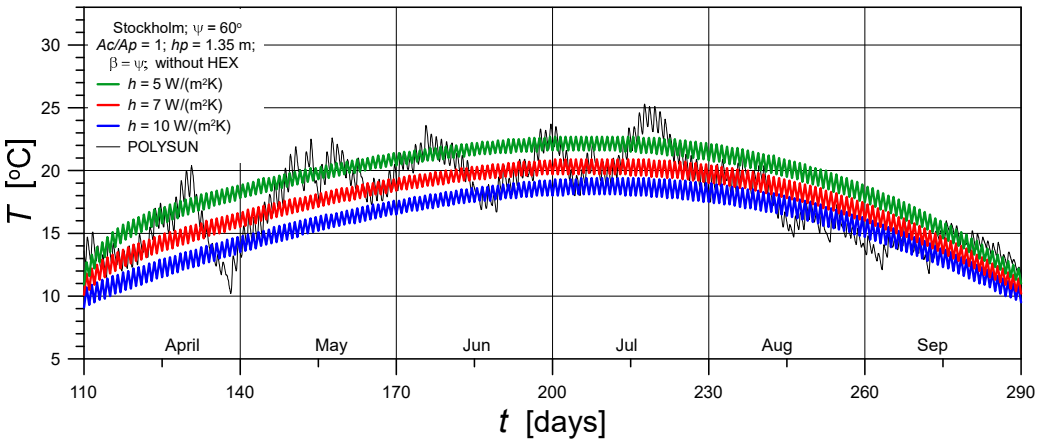

Figure 10. Time curves of T_p calculated by the proposed model and POLYSUN for Stockholm.

For an approximate quantitative analysis of the results, the concept of a control parameter was introduced, defined here as the h. Although this is not the only variable subject to random variation, it is likely the one whose fluctuations have the greatest impact on the water temperature profile. Table 6 presents the ranges of h values and the corresponding approximate average values for which the discrepancies between the calculation results are minimal. The table also shows the maximum daytime and nighttime water temperatures recorded at each location.

Table 6. Selected results of solar water heating system simulations in various locations.

Parameter	Thesaloniki	Krakow	Stockholm
Range of h [W/(m²K)]	5-11	7-13	5-10
Average h [W/(m²K)]	8	10	7
Maximum T_p at day [°C]	29.5	24.8	20.9
Maximum T_p at night [°C]	27.1	22.2	19.7

4.2. The Effect of A_c on T_p

Starting from this chapter, all the drawings considered concern Krakow. The effect of collector area on solar pool water heating is best represented by the dimensionless ratio of collector area to pool area, A_c/A_p. This is a key parameter in the process under consideration. Figure 11 shows the temperature curves for several values of the A_c/A_p ratio, as well as for the case without solar collector heating (A_c/A_p= 0). The results clearly demonstrate that increasing A_c leads to a systematic rise in T_p over the entire analyzed period. Even a relatively small A_c/A_p ratio results in a noticeable temperature increase compared to the reference case. The differences between the curves are most evident during the summer months (June–August), when solar radiation intensity is highest. In this period, larger A_c enable T_p to exceed 25°C, while in the absence of solar heating, the temperature remains at a substantially lower level. This indicates that A_c not only affects peak temperatures but also extends the duration of favorable thermal conditions for pool use. It was found that, under Krakow's conditions, installing solar collectors with a surface area half that of the pool surface area makes it possible to maintain the water temperature (during the day) above 21°C for 100 days.

 doi:10.20944/preprints202603.1893.v1

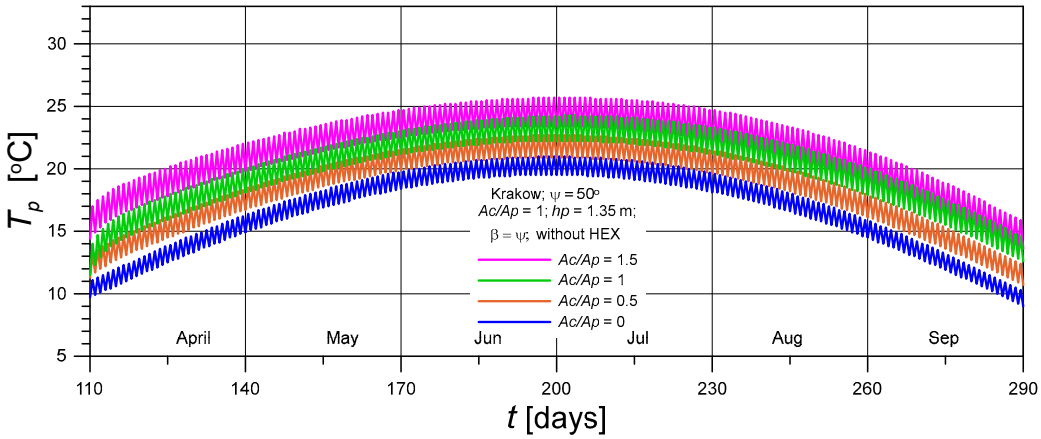

Figure 11. The effect of the A_c/A_p ratio on the temporal variation of T_p values.

4.3. Heat Losses from Pool Water to the Environment

Figure 12 shows the heat fluxes transported from the pool water surface to the surroundings. The largest contribution to heat loss comes from EV and LW. The latter flux is uniform over time, while the EV has a strong maximum during the warmest period. The flux changes during the night/day periods are significant for EV, while they are small for the LW. H_{conv} is smaller than previously mentioned and exhibits significant day-to-night flux variations.

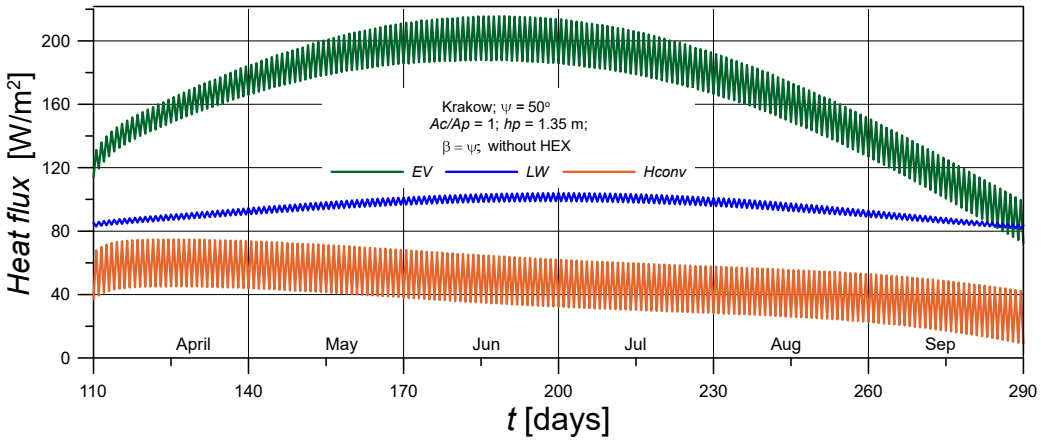

Figure 12. Heat losses from the water surface.

4.4. Preventing Heat Losses from the Water's Surface

Under the assumption that individual heat losses to the environment were eliminated T_p values were analyzed. In practice, however, such losses can only be partially reduced. The purpose of these calculations was to demonstrate the theoretical potential for minimizing heat losses. Nevertheless, certain practical measures—such as the periodic (nighttime) use of pool covers and the construction of pools in sheltered locations—can significantly reduce these losses.

The application of a cover on the water surface effectively limits evaporation and reduces long-wave radiative heat losses. In the model, complete elimination of evaporation can be simulated by setting $A = 0$ in Eq. (23), while suppression of LW is achieved by assuming a water emissivity coefficient of $\varepsilon = 0$ in Eq. (21). For both cases, the resulting water temperature profiles, corresponding to the elimination of these heat flux components, are presented in Figure 13.

 doi:10.20944/preprints202603.1893.v1

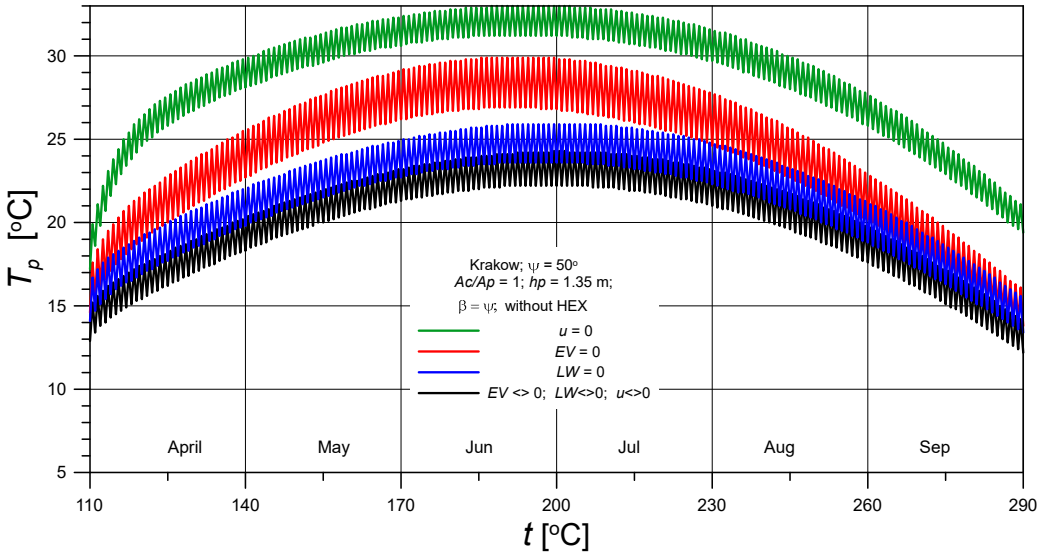

Figure 13. Potential ways to reduce heat losses in solar pool water heating system.

As noted, the dominant mechanisms of heat losses in the pool are EV and LW. Nevertheless, the mitigation of convective heat transfer remains of considerable importance. This effect is illustrated by the uppermost curve in Figure 13, which was obtained by substituting $u = 0$ into Eq. (20). A substantial reduction in overall heat loss can be achieved by locating the pool in a wind-sheltered environment. Within the framework of the model, this condition corresponds to zero wind velocity, for which h assumes a significantly lower—albeit non-zero—value, characteristic of free convection.

A reduction in wind speed yields additional benefits beyond the decrease in H_{conv}:

- EV is also reduced, due to the analogy between heat and mass transfer, whereby the heat transfer coefficient occurs on Eq. (19),
- for a wind-sheltered pool, a decrease in heat loss is observed under both daytime and nighttime conditions.

4.5. Solar System with a Heat Exchanger

Figure 1 presents the system layout with and without a heat exchanger, while Figure 14 illustrates the corresponding temperature profiles for the system with a heat exchanger. The calculations were performed for a heat exchanger with a parameter $(UA)_{HEX} = 1000$ W/K and for solar fluid flow rates of 0.1 and 0.3 kg/s, corresponding to NTU values of 0.8 and 2.4, respectively. An increase in the water flow rate results in a lower temperature at the inlet to the pool T_c. At the same time, higher flow rates reduce the temperature difference between the inlet and outlet of the heat exchanger, leading to an increase in the temperature at the collector inlet T_p'. This temperature, in turn, affects the collector's efficiency.

The temperature profiles of T_c, T_p, and T_p' are shown in Figure 14. The water flow rate has a strong influence on T_c profile and a less pronounced effect on T_p'. However, within the analyzed range and for constant value of $(UA)_{HEX}$ the flow rate through the heat exchanger does not significantly affect T_p.

The behavior of the utilizability parameter used in the model was also analyzed. As shown in Figure 14, the values of ϕ remain close to unity and are nearly constant over time. They are slightly higher for lower water flow rates, which can be explained by the higher collector inlet temperature under these conditions, resulting in a reduced driving force for heat transfer in the collector. The fact that ϕ remains close to unity is due to two main reasons. First, in the present model, collector operation is limited to daytime, so the absence of solar radiation at night does not influence the value of ϕ. The second reason is that the analysis covers only the summer period, which means that ϕ is not affected by the low heat fluxes that occur in winter.

 doi:10.20944/preprints202603.1893.v1

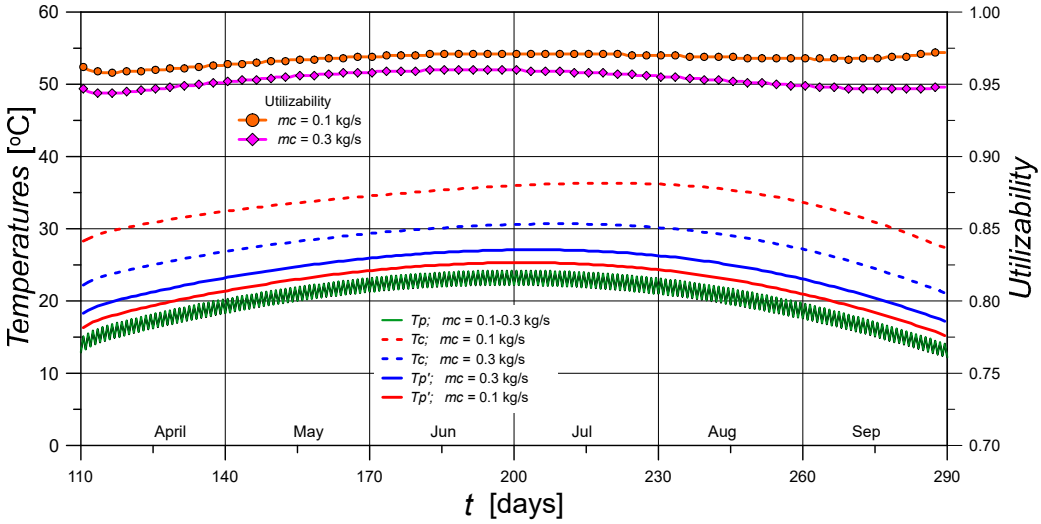

Figure 14. Temperature profiles and ϕ values for solar pool heating with a heat exchanger.

5. Conclusions

The present study investigated the performance of a solar pool water heating system using both a simplified analytical model and numerical simulations in POLYSUN. Analysis of the calculation results allows the formation of the following conclusions:

1. Solar heating with a properly designed heat exchanger yields thermal performance comparable to that achieved by direct circulation of water from the collector to the pool. This has been demonstrated for heat exchangers with NTU values 0.8 and 2.4.
2. Increasing the collector area leads to higher pool water temperatures; however, the applicability of this approach is limited by economic and spatial constraints.
3. In high-latitude regions (e.g., 60°), solar pool water heating alone is insufficient to ensure acceptable water temperature conditions.
4. Minimizing heat losses to the environment is crucial in solar pool water heating systems. Wind speed has been identified as a key factor influencing these losses. Locating the pool in a sheltered, low-wind area reduces both convective and evaporative heat losses. Moreover, such a solution is effective continuously, both during the day and at night, unlike the intermittent use of pool covers.
5. A solar heating model was developed based on dividing each day into two periods—daytime and nighttime—separated by sunrise and sunset. When combined with the concept of utilizability, this approach yields a simple model that provides an adequate representation of the real process. Although it does not capture short-term variations due to the use of smoothed weather data, it successfully reproduces the overall temperature trends and can be used as a practical tool for preliminary design and analysis.
6. The use of the proposed model to simulate solar water heating in a pool confirmed its suitability. A comparison with the results obtained from the POLYSUN application showed good agreement under various climatic conditions in Europe.

Author Contributions: Conceptualization, K.K. and S.P.; methodology, K.K.; software, K.K. and S.P.; validation, K.K.; formal analysis, K.K. and S.P.; investigation, K.K. and S.P.; resources, K.K. and S.P.; data curation, K.K. and S.P.; writing—original draft preparation, K.K. and S.P.; writing—review and editing, K.K. and S.P.; visualization, K.K. and S.P.; supervision, K.K. and S.P.; project administration, K.K. and S.P. All authors have read and agreed to the published version of the manuscript.

Funding: This research received no external funding.

Institutional Review Board Statement: Not applicable.

 doi:10.20944/preprints202603.1893.v1

Informed Consent Statement: Not applicable.

Data Availability Statement: The data used in this study can be obtained from the corresponding author upon request.

Conflicts of Interest: The authors declare no conflicts of interest.

Nomenclature

A_c	solar collectors' surface area, m²;
A_p	pool surface area, m²;
B_d	daily temperature amplitude, K or °C;
c	heat capacity, J/(kgK);
EV	evaporative heat flux, W/m²;
F_R	collector heat removal factor;
h	heat transfer coefficient, W/(m²K);
H	daily radiation on the horizontal surface, J/m²;
H_{conv}	convective heat flux, W/m²;
H_T	daily insolation on a tilted surface, J/m²;
h_p	pool deep, m;
I_{Tc}	critical solar radiation intensity, W/m²;
K_T	clearness index;
LW	long-wave radiation flux, W/m²;
n	day of the year;
NTU	Number of Transfer Units;
$\dot{m}_p$	water flow rate in the pool circuit, kg/s;
Q_{in}	amount of heat supplied to the water in the pool during day, J;
Q_{out}	amount of heat pool losses during the day, J;
Q_p	daily useful heat transferred to the pool system, J;
PVGIS	Photovoltaic Geographical Information System;
R	coefficient of daily heat transfer from the horizontal surface to the inclined surface;
R_b	ratio of daily beam radiation on a tilted surface to that on a horizontal surface;
RH	relative air humidity;
R_n	monthly average ratio of total radiation on the tilted plane to that on the horizontal plane;
$r_{t,n}$	ratio of total radiation in an hour to total in a day (noon);
SC	solar collector;
t_1, t_2	the beginning and end time of the daily period;
T	temperature, °C;
T_a	average daily air temperature, °C;
T_{an}	average water temperature for night period, °C;
T_{ad}	average water temperature for day period, °C;
T_c	outlet solar fluid temperature in solar collector, °C;
T_d	daily average air temperature during the day, °C;
T_n	daily average air temperature during the night, °C;
T_p	pool water temperature, K or °C;
T_p'	temperature at the outlet of the exchanger, °C;
T_{sky}	sky temperature, K;
u	wind speed, m/s;
V_p	water volume in the pool, m³;
Δt	the length of the day, h; time step (= 1 day);
Δt_d	the length of the day, h; time step (= 1 day);
$(\tau\alpha)$	effective transmittance – absorptance product;
β	collectors slope, rad or °;
ε	emissivity of the water surface;
ρ	water density, kg/m³;
ρ_g	diffuse reflectance;
σ	Stefan-Boltzmann constant, 5.67×10^{-8} W m^{-2} K^{-4};
ϕ	daily utilizability;

 doi:10.20944/preprints202603.1893.v1

ψ latitude, rad or °;
ω frequency, 2π/365;
ω_d frequency, 2π/24;
ω_s sunset (or sunrise) hour angle, rad;

References

1. Gonçalves, R.S.; Palmero-Marrero, A.I.; Oliveira, A.C. Analysis of Swimming Pool Solar Heating Using the Utilizability Method. *Energy Reports* **2020**, *6*, 717–724, doi:10.1016/j.egyr.2019.09.055.
2. Buscemi, A.; Biondi, A.; Catrini, P.; Guarino, S.; Lo Brano, V. A Novel Model to Assess the Energy Demand of Outdoor Swimming Pools. *Energy Convers. Manag.* **2024**, *302*, 118152, doi:10.1016/j.enconman.2024.118152.
3. Li, Y.; Nord, N.; Huang, G.; Li, X. Swimming Pool Heating Technology: A State-of-the-Art Review. *Build. Simul.* **2021**, *14*, 421–440, doi:10.1007/s12273-020-0669-3.
4. Ruiz, E.; Martínez, P.J. Analysis of an Open-Air Swimming Pool Solar Heating System by Using an Experimentally Validated TRNSYS Model. *Sol. Energy* **2010**, *84*, 116–123, doi:10.1016/j.solener.2009.10.015.
5. Lugo, S.; Morales, L.I.; Best, R.; Gómez, V.H.; García-Valladares, O. Numerical Simulation and Experimental Validation of an Outdoor-Swimming-Pool Solar Heating System in Warm Climates. *Sol. Energy* **2019**, *189*, 45–56, doi:10.1016/j.solener.2019.07.041.
6. Zhao, J.; Bilbao, J.I.; Spooner, E.D.; Sproul, A.B. Experimental Study of a Solar Pool Heating System under Lower Flow and Low Pump Speed Conditions. *Renew. Energy* **2018**, *119*, 320–335, doi:10.1016/j.renene.2017.12.006.
7. Cunio, L.N.; Sproul, A.B. Performance Characterisation and Energy Savings of Uncovered Swimming Pool Solar Collectors under Reduced Flow Rate Conditions. *Sol. Energy* **2012**, *86*, 1511–1517, doi:10.1016/j.solener.2012.02.012.
8. Kupiec, K.; Pater, S. On the Possibility of Achieving High Solar Fractions for Space Heating in Temperate Climates. *Sol. Energy* **2025**, *300*, doi:10.1016/j.solener.2025.113789.
9. Starke, A.R.; Cardemil, J.M.; Colle, S. Multi-Objective Optimization of a Solar-Assisted Heat Pump for Swimming Pool Heating Using Genetic Algorithm. *Appl. Therm. Eng.* **2018**, *142*, 118–126, doi:10.1016/j.applthermaleng.2018.06.067.
10. Li, Y.; Liang, J.; Chen, W.; Wu, Z.; Yin, H. Optimal Design of a Solar-Assisted Heat Pump System with PCM Tank for Swimming Pool Utilization. *Renew. Energy* **2025**, *240*, 122272, doi:10.1016/j.renene.2024.122272.
11. Ren, C.; Lin, J.; Guo, N. Performance and Optimization of Novel Solar-Assisted Heat Pump System with Hybrid Thermal Energy Storage. *Energies* **2024**, *17*, 5944, doi:10.3390/en17235944.
12. Sezen, K.; Gungor, A. Comparison of Solar Assisted Heat Pump Systems for Heating Residences: A Review. *Sol. Energy* **2023**, *249*, 424–445, doi:10.1016/j.solener.2022.11.051.
13. Luo, C.; Peng, J.; Chen, X.; Su, X.; El Shenawy, E.T.; Ji, J.; Jiang, Q.; Peng, R.; Zhang, H. Thermal Dynamics and Energy Performance of Open Solar Photovoltaic/Thermal Pool System: Experimental and Theoretical Study. *Appl. Therm. Eng.* **2025**, *279*, 127763, doi:10.1016/j.applthermaleng.2025.127763.
14. Katsaprakakis, D. Introducing a Solar-Combi System for Hot Water Production and Swimming Pools Heating in the Pancretan Stadium, Crete, Greece. *Energy Procedia* **2019**, *159*, 174–179, doi:10.1016/j.egypro.2018.12.047.
15. Mardi, M. El; Allouhi, A.; Rami, Y.; Tabet Aoul, K.A. Cost-Effective and Sustainable Heating Solutions for Indoor Swimming Pools: A Comparative Study and LCOH Assessment of PV-Heat Pumps and Solar Thermal Collectors. *Energy Nexus* **2025**, *18*, doi:10.1016/j.nexus.2025.100414.
16. Bergman, T.L.A.S.L. *Fundamentals of Heat and Mass Transfer*; 8th editio.; John Wiley & Sons Inc.: Hoboken, NJ, USA, 2017; ISBN 9781119320425.
17. Duffie, J.A.; Beckman, W.A. *Solar Engineering of Thermal Processes*; Fourth.; John Wiley & Sons: Hoboken, NJ, USA, 2013; ISBN 978-0-470-87366-3.
18. European Commission Photovoltaic Geographical Information System Available online: https://re.jrc.ec.europa.eu/pvg_tools/en/ (accessed on 12 March 2026).

 doi:10.20944/preprints202603.1893.v1

19. Chiasson, A.D. *Geothermal Heat Pump and Heat Engine Systems: Theory and Practice*; John Wiley & Sons, Ltd.: Hoboken, NJ, USA, 2016; ISBN 9781118961940.
20. Perry, R.H.; Green, D.W.; Maloney, J.O. *10. Transport and Storage of Fluids*; The McGraw-Hill Companies Inc.: Columbus, OH, USA, 1997; ISBN 0070498415.
21. Pater, S.; Kupiec, K. Improving Thermal Performance of Solar Heating Systems. *Appl. Sci.* **2025**, *15*, 11118, doi:10.3390/app152011118.
22. Vela Solaris AG POLYSUN Designer Available online: https://www.velasolaris.com/ (accessed on 22 March 2026).